CHEMISTRY
AN ASIAN JOURNAL
ACES
FULL PAPER

DOI: 10.1002/asia.201301638

PdO/TiO_2 and Pd/TiO_2 Heterostructured Nanobelts with Enhanced Photocatalytic Activity

Weijia Zhou,[a, b] Yu Guan,[a] Dongzhou Wang,[a] Xinhai Zhang,[c] Duo Liu,[a] Huaidong Jiang,[a] Jiyang Wang,[a] Xiaogang Liu,[d] Hong Liu,*[a] and Shaowei Chen[b]

Abstract: Heterostructures play an important role not only in the manufacture of semiconductor devices, but also in the field of catalysis. Herein, we report the synthesis of PdO/TiO_2 and Pd/TiO_2 heterostructured nanobelts by means of a simple co-precipitation method, followed by a reduction process using surface-modified TiO_2 nanobelts as templates. The as-obtained heterostructures were characterized by transmission electron microscopy, X-ray photoelectron spectroscopy, and UV/Vis diffuse reflectance spectroscopy. PdO and Pd nanoparticles with a size of about 1.3 and 1.6 nm were assembled uniformly on the surface of TiO_2 nanobelts, respectively. Compared with TiO_2 nanobelts, PdO/TiO_2 and Pd/TiO_2 hybrid nanobelts exhibit enhanced photocatalytic activity upon UV and visible-light irradiation. Photoelectrochemical technology was used to study the heterostructure effect on enhanced photocatalytic activity. Our mechanistic investigation revealed that energy-band matching is the major factor in the observed enhancement of photocatalytic activity.

Keywords: heterostructures · palladium · photochemistry · nanostructures · titanium

Introduction

One-dimensional (1D) semiconducting metal oxide nanostructures with large surface-to-volume ratios have become the focus of intensive research, as they provide an excellent platform for investigating shape- or size-dependent electrical and thermal transport properties. In particular, 1D semiconducting oxide nanostructures (TiO_2, ZnO, SnO_2, CeO_2, Co_3O_4, $W_{18}O_{49}$) such as nanotubes (NTs),[1,2] nanobelts (NBs),[3,4] nanowires (NWs),[5,6] and nanorods (NRs)[7,8] have attracted considerable attention owing to their unique physical and chemical properties. Titanium dioxide (TiO_2) is a technologically important material that has many promising applications in areas that range from photocatalysis[9,10] to solar cells[11,12] and sensors.[13,14] The movement of electrons and holes in TiO_2 semiconductor nanomaterials is primarily governed by 1D quantum confinement.[15] However, the photocatalytic activity of TiO_2 nanobelts is relatively low owing to their fewer surface active sites and high recombination of photogenerated electron–hole pairs.[16] Clearly, the improvement of the photocatalytic ability of TiO_2 nanobelts is an important issue that needs to be addressed prior to their applications in photocatalysis.

The growth of heterostructures is one of the most important approaches for the development of advanced multifunctional nanomaterials.[17–19] Recently, the fabrication of heterostructures on the surface of 1D metal oxide, such as semiconductors (SnO_2, MoS_2, and CdS)[20–22] and noble metals,[23–25] has attracted a great deal of research interest. Liu and co-workers fabricated the controllable binary TiO_2/SnO_2 nanofibers with enhanced photocatalytic activity.[20] Kolmakov et al. reported that the deposition of Pd nanoparticles on SnO_2 nanowires enabled the generation of Schottky barrier-type junctions with dramatically improved sensitivity toward sensing of oxygen and hydrogen gases.[26] On the basis of these recent works, it is evident that heterostructures can effectively modulate charge transfer between two phases to improve the catalytic performance. The TiO_2 nanobelt is a good substrate owing to its dimensionally and structurally well-defined physical and chemical phenomena. At the same time, the rough surface of TiO_2 nanobelts obtained by acid hydrothermal corrosion (referred to as C-TiO_2) is ideal as a template for heterogeneous nucleation of metal or metal oxide nanoparticles.

[a] Dr. W. Zhou, Y. Guan, D. Wang, Prof. D. Liu, Prof. H. Jiang, Prof. J. Wang, Prof. H. Liu
State Key Laboratory of Crystal Materials
Center of Bio&Micro/Nano Functional Materials
Shandong University, 27 South Shanda Road
Jinan 250100 (China)
E-mail: hongliu@sdu.edu.cn

[b] Dr. W. Zhou, Prof. S. Chen
New Energy Research Center, School of Environment and Energy
South China University of Technology, University Town
Guangzhou 510006 (China)

[c] Prof. X. Zhang
Department of Electrical and Electronic Engineering
South University of Science and Technology of China
Tangchang Rd., Xili, Nanshan District
Shenzhen, 518055 (China)

[d] Prof. X. Liu
Department of Chemistry, National University of Singapore
3 Science Drive 3, 117543 (Singapore)

Supporting information for this article is available on the WWW under http://dx.doi.org/10.1002/asia.201301638.

In this work, we report the fabrication of PdO/C-TiO_2 and Pd/C-TiO_2 heterostructured nanobelts by a co-precipitation method followed by a reduction process. The uniform distribution of palladium oxide (PdO) and palladium (Pd) nanoparticles on the surface of C-TiO_2 nanobelts was observed by transmission electron microscopy (TEM), X-ray photoelectron spectroscopy (XPS), and UV/Vis absorption spectroscopy. The photocatalytic activity and photocurrent were characterized to study the heterostructure effect. We also present a mechanistic investigation on PdO/C-TiO_2 and Pd/C-TiO_2 nanobelt heterostructures that suggest the energy-band matching is the dominant factor for the enhanced photocatalytic activity of nanoparticle-modified TiO_2 nanobelts.

Results and Discussion

As reported in our previous study,[23] smooth nanobelts (referred to as TiO_2) and coarse nanobelts (referred to as C-TiO_2) were synthesized by means of an alkali hydrothermal method followed by an acid corrosion process (see the Supporting Information). The thickness of the nanobelts is about 20 nm, the width is 50–300 nm, and the length is up to several tens of micrometers. TEM images of Pd/C-TiO_2 and PdO/C-TiO_2 heterostructured nanobelts are shown in Figure 1. Anatase nanobelts obtained by acid corrosion treatment have a rough surface (see the Supporting Information), which is beneficial to the heterogeneous nucleation of PdO nanoparticles on the surface of C-TiO_2 nanobelts during the co-precipitation process. Small PdO nanoparticles with a diameter of (1.3 ± 0.4) nm were observed, which were evenly distributed on the surface of C-TiO_2 nanobelts (Figure 1a,c). After the reduction reaction, the average particle size of Pd nanoparticles deposited onto the nanobelts was found to be slightly increased, which was about (1.6 ± 0.5) nm (Figure 1b,d). The corresponding size distributions of PdO and Pd nanoparticles on C-TiO_2 nanobelts are shown in the Supporting Information, respectively. Thus, we presumed that the reduction reaction from PdO nanoparticles to Pd nanoparticles is a dissolution–recrystallization process.[27] It is worth noting that the PdO and Pd nanoparticles were firmly integrated on C-TiO_2 nanobelts and not leached off even after ultrasonic treatment. Because of their low content (2 wt%) and small size, the PdO and Pd nanoparticles were not observed by XRD (see the Supporting Information). However, the existence of elemental Pd in the PdO/C-TiO_2 and Pd/C-TiO_2 hybrid nanobelts with loading contents of 1.7 and 1.65 wt%, respectively, was confirmed by EDS analysis (see the Supporting Information). To confirm the crystalline phase of the heterostructures, increased amounts (8 wt%) of PdO and Pd were loaded onto C-TiO_2 nanobelts. The TEM imaging and XRD characterization are shown in the Supporting Information. However, only bumps at 34 and 40° were observed in the XRD pattern of PdO/C-TiO_2 and Pd/C-TiO_2, respectively, which correspond to PdO (JCPDS 43-1024, tetragonal, $a=b=0.3$ nm, $c=0.54$ nm) and Pd (JCPDS 65-2867, cubic, $a=b=c=0.39$ nm). The crystal lattices of the PdO and Pd nanoparticles can be seen in Figure 1c and d, respectively. The interplanar distances of 0.35 (Figure 1c), 0.24, and 0.19 nm (Figure 1d) correspond to the (101), (004), and (200) crystal planes of anatase TiO_2, which implies that the growth front of TiO_2 nanobelt is the (101) plane. The fringe spacing of 0.26 nm (Figure 1c) corresponds to the (101) planes for PdO nanoparticles. The lattice spacing of Pd nanoparticles closely matches that of the bulk metal, which is 0.22 nm for the (111) crystal plane of Pd. The PdO and Pd nanoparticles are tightly coupled to the surface of C-TiO_2 nanobelts to form PdO/C-TiO_2 and Pd/C-TiO_2 heterostructures, which is important for facilitating charge transfer.

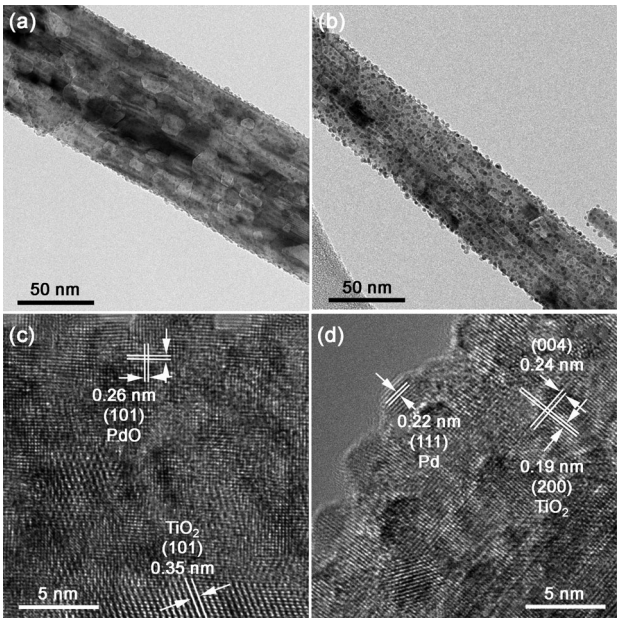

Figure 1. a,b) TEM images of C-TiO_2 nanobelts modified with PdO and Pd nanoparticles, respectively. c,d) The corresponding high-resolution TEM images of PdO/C-TiO_2 (2 wt%) and Pd/C-TiO_2 nanobelts.

XPS measurements revealed the presence of elemental Ti, O, Pd, and C in PdO/C-TiO_2 and Pd/C-TiO_2 nanobelt heterostructures (Figure 2). The C is ascribed to the adventitious hydrocarbon from the XPS instrument itself. The high-resolution XPS spectra show that the banding energies of $Pd3d_{5/2}$ and $Pd3d_{3/2}$ in the PdO/C-TiO_2 nanobelts are located at 337.35 and 342.65 eV, respectively, which suggest that Pd existed as Pd^{2+} in the PdO/C-TiO_2 nanobelt heterostructures. After the reducing reaction, the binding energies for $Pd3d_{5/2}$ and $Pd3d_{3/2}$ for the Pd/C-TiO_2 nanobelts were observed at 334.4 and 339.9 eV, thereby implying the presence of elemental Pd^0. The asymmetric peaks for $Pd3d_{5/2}$ and $Pd3d_{3/2}$ for the reduced nanobelts suggest partial surface oxidation of Pd nanoparticles, typically observed for small Pd nanoparticles.

To test the photocatalytic activity of PdO/C-TiO_2 and Pd/C-TiO_2 nanobelts, methyl orange (MO), methyl blue, rhodamine B, and *p*-chlorophenol were chosen as they are commonly found in most organic dyes. The photocatalytic activi-

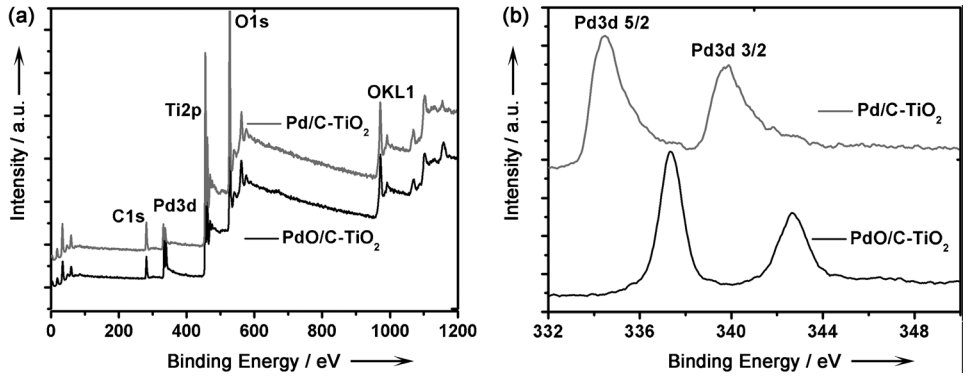

Figure 2. a) XPS survey spectra of PdO/C-TiO_2 and Pd/C-TiO_2 nanobelts. b) XPS spectra of the samples showing the $Pd3d_{5/2}$ and $Pd3d_{3/2}$ peaks.

ty of C-TiO_2 nanobelts decorated with PdO and Pd nanoparticles is shown in Figure 3. Under UV-light irradiation, the photocatalytic performance of common variety TiO_2 nanobelts was poor, and the decomposition of MO only approached 53.6% after UV-light irradiation for 20 min (Figure 3a). The photocatalytic performance of C-TiO_2 nanobelts treated with acid corrosion was improved drastically, and the degree of MO decomposition increased to 76.8% in 20 min. The result is attributed to the higher Brunauer–Emmett–Teller (BET) surface area of C-TiO_2 nanobelts, which increased from 20.78 $m^2 g^{-1}$ for TiO_2 nanobelts to 29.13 $m^2 g^{-1}$ for C-TiO_2 nanobelts. After the attachment of PdO nanoparticles onto the surface of C-TiO_2 nanobelts, the resulting PdO/C-TiO_2 nanobelts gave rise to enhanced photocatalytic activity. A complete degradation of MO was achieved in 20 min, which was significantly higher than that of C-TiO_2 nanobelts and P25 (a commercial TiO_2 photocatalyst). In contrast to PdO/C-TiO_2 nanobelts, the photocatalytic activity of Pd/C-TiO_2 nanobelts obtained by reduction reaction was slightly decreased to 97.5%. However, the photocatalytic activity of Pd/C-TiO_2 nanobelts was also higher than that of the C-TiO_2 nanobelts. Through a zero-order linear fitting, the decomposition rates of MO for the PdO/C-TiO_2 (0.0415 mg min^{-1}) and Pd/C-TiO_2 (0.03 mg min^{-1}) nanobelts were measured to be more than threefold and 2.1-fold faster than that (0.014 mg min^{-1}) of the TiO_2 nanobelts, respectively. Through a first-order linear fitting, the k values for TiO_2 nanobelts, PdO/C-TiO_2 and Pd/C-TiO_2 nanobelts, and P25 are 0.0178, 0.03, 0.513, 0.997, and 0.033, respectively, which also implied that the enhanced photocatalytic performance was caused by a heterostructure effect. UV photocatalytic activity of the heterostructures with different loading content of PdO and Pd nanoparticles is shown in the Supporting Information.

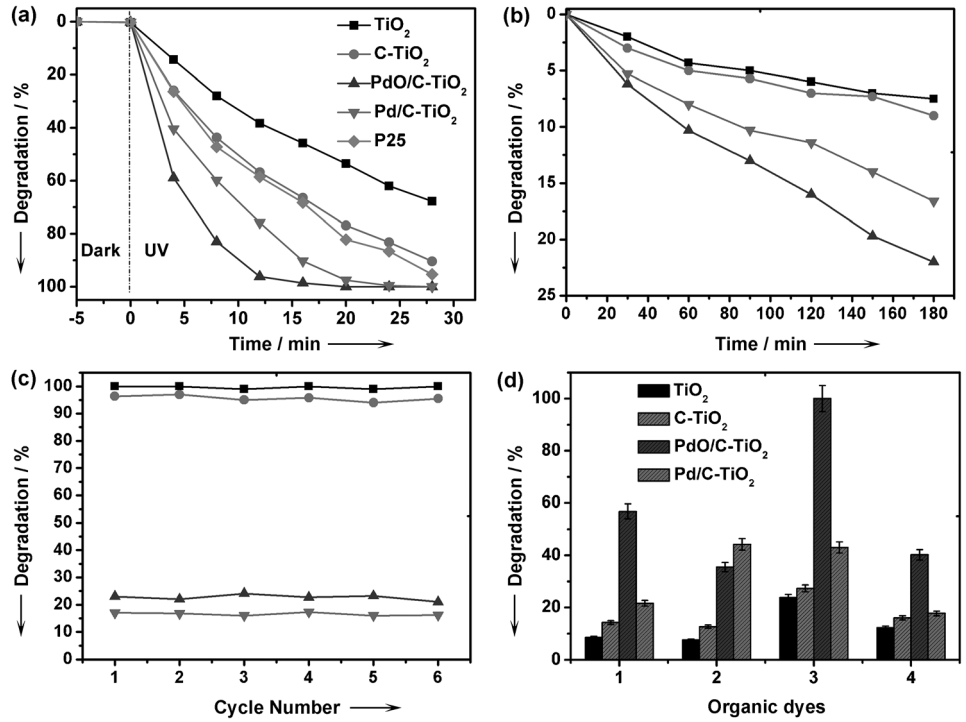

Figure 3. Photocatalytic degradation of methyl orange (MO) in the presence of TiO_2 nanobelts, C-TiO_2 nanobelts, PdO/C-TiO_2 and Pd/C-TiO_2 nanobelt heterostructures, and P25 under a) UV light and b) visible-light irradiation. c) Irradiation time dependence of photocatalytic degradation of MO in aqueous solutions over PdO/C-TiO_2 and Pd/C-TiO_2 nanobelt heterostructures during repeated photo-oxidation experiments under UV (20 min) and visible-light irradiation (180 min). d) Photocatalytic degradation of methyl orange (labeled as 1), methylene blue (labeled as 2), rhodamine B (labeled as 3), and *p*-chlorophenol (labeled as 4) in the presence of TiO_2 nanobelts, C-TiO_2 nanobelts, and PdO/C-TiO_2 and Pd/C-TiO_2 nanobelt heterostructures under UV-light irradiation for 4 min.

The visible-light photocatalytic activity of TiO_2 nanobelts, C-TiO_2 nanobelts, and PdO/C-TiO_2 and Pd/C-TiO_2 nanobelt heterostructures was also evaluated by photocatalytic degradation of MO in aqueous solution under visible-light irradiation (Figure 3b). Owing to the large bandgap energy (about 3.2 eV for anatase), the photocatalysis of TiO_2 nanobelts only proceeds at wavelengths shorter than approximately 400 nm. Hence, the TiO_2 and C-TiO_2 nanobelts have low photocatalytic activity under visible-light

irradiation, and the degradation rates are only 7.5 and 9% over 180 min, respectively. The photocatalytic activities of the PdO/C-TiO_2 and Pd/C-TiO_2 nanobelt heterostructures are better than that of the pure TiO_2 nanobelts. The corresponding degradation rates of MO reach 22 and 16.6% under the same conditions, respectively.

The UV/Vis absorption spectra of TiO_2 nanobelts, C-TiO_2 nanobelts, and PdO/C-TiO_2 and Pd/C-TiO_2 nanobelt heterostructures were used to support the visible-light photocatalytic activity results (Figure 4). TiO_2 nanobelts exhibit

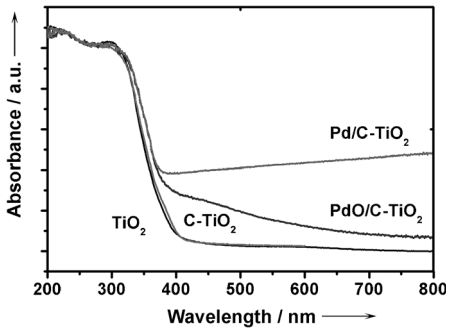

Figure 4. UV-visible absorption spectra of TiO_2 nanobelts, C-TiO_2 nanobelts, and PdO/C-TiO_2 and Pd/C-TiO_2 nanobelt heterostructures.

a steep absorption edge located at about 380 nm and are consistent with the intrinsic bandgap absorption of pure anatase TiO_2 (about 3.2 eV). PdO/C-TiO_2 nanobelt heterostructures show a strong and wide absorption band in the visible-light region (from 400 to 550 nm), whereas Pd/C-TiO_2 nanobelt heterostructures exhibit the visible-light absorption band from 400 nm to the near-infrared region. When the amount of PdO loading was increased from 1 to 12 wt%, the photocatalytic degradation rate changed from 12.3 to 25.6% (see the Supporting Information). Unlike PdO/C-TiO_2, with the same amount of increase in the Pd loading content, the photocatalytic degradation was improved from 6.5 to 39.6% (see the Supporting Information). The results were consistent with UV-visible absorption spectra, which suggests that the ability of PdO and Pd nanoparticles to sensitize visible light is key to the enhancement of the photocatalytic activity of the TiO_2 nanobelt.

To investigate the photocatalytic stability of the PdO/C-TiO_2 and Pd/C-TiO_2 heterostructured nanobelts, the catalysts were separated by membrane filtration, recycled, and reused six times. Evidently, the PdO/C-TiO_2 and Pd/C-TiO_2 nanobelts exhibit very stable photocatalytic activity under UV and visible-light irradiation (Figure 3c). There was no significant decrease in the decomposition rate of MO after six cycles. Although commercial titania P25 has been reported to be effective for the photocatalytic degradation of various organic contaminants in aqueous solution, their practical use in aqueous media is limited because of the technical difficulty of filtration and the recovery of small-sized TiO_2 particles. In contrast, TiO_2 nanobelts can be easily recovered from the dye solution on account of the 1D structure.[17] Figure 3d shows the degradation results of methyl orange, methylene blue, rhodamine B, and *p*-chlorophenol in the presence of TiO_2 nanobelts, C-TiO_2 nanobelts, and PdO/C-TiO_2 and Pd/C-TiO_2 nanobelt heterostructures upon irradiation with UV light for 4 min. It can be seen that the as-synthesized PdO/C-TiO_2 nanobelts show a high photocatalytic activity for all organic dyes under investigation. The molecular structures and corresponding UV/Vis absorption spectra of the dyes are shown in the Supporting Information.

To further understand the heterostructure effect on the photocatalytic activity, we studied the photoinduced charge-transfer properties of C-TiO_2, PdO/C-TiO_2, and Pd/C-TiO_2. Photographs of ITO photoelectrodes composed of C-TiO_2, PdO/C-TiO_2, and Pd/C-TiO_2 are shown in the Supporting Information. Figure 5a and b show that PdO/C-TiO_2 and Pd/C-TiO_2 generate a higher photocurrent than that of C-TiO_2 nanobelts under both UV and visible-light irradiation. The obtained photocurrent result is consistent with the UV and visible photocatalytic activity of TiO_2 nanobelt heterostructures (Figure 3). The enhanced UV photocurrent of PdO/C-

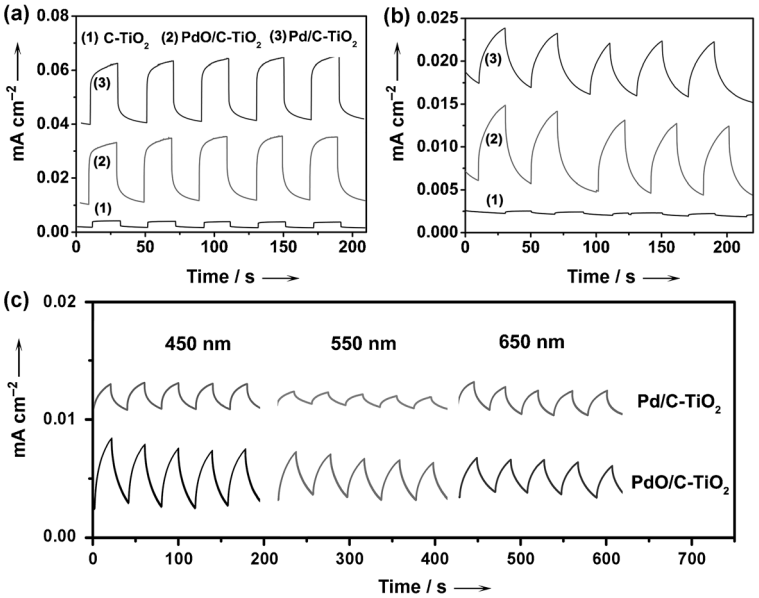

Figure 5. Time-dependent photocurrent response of the ITO photoelectrodes composed of C-TiO_2, PdO/C-TiO_2, and Pd/C-TiO_2, respectively, at a bias voltage of 0.5 V. All the photocurrent intensities were normalized to the dark current. a) UV-light irradiation, b) visible-light irradiation, and c) monochromatic light irradiation at 450, 550, and 650 nm, respectively.

TiO_2 and Pd/C-TiO_2 is attributed to the inhibition of the photo-produced electron/hole (e^-/h^+) recombination by energy-band matching and the Schottky barrier effect. Under visible-light irradiation, C-TiO_2 nanobelts show a negligible photocurrent, and the high photocurrent of PdO/C-TiO_2 and Pd/C-TiO_2 was produced from the sensitizing effect of PdO and Pd nanoparticles. To clarify the detailed sensitizing effect, monochromatic lights of 450, 550, and 650 nm were used as a light source to study the relationship of photocurrent and wavelength, which is shown in Figure 5c. For PdO/C-TiO_2, the highest photocurrent was obtained under 450 nm-light irradiation, which is consistent with the UV-visible absorption spectra of PdO/C-TiO_2 in which the strong absorption band at about 450 nm was observed (Figure 4). Surprisingly, the lowest photocurrent obtained by 550 nm-light irradiation among the three irradiation wavelengths was for Pd/C-TiO_2. The high photocurrent of Pd/C-TiO_2 under 450 nm can be attributed to the plasmonic effect of Pd nanoparticles on the C-TiO_2 nanobelt, which can cause the Fermi level of C-TiO_2 to shift toward more positive potentials, and finally effectively capture the visible light ($\geq$420 nm).[28–31] As for the high photocurrent of Pd/C-TiO_2 under 650 nm irradiation, the result is consistent with the UV-visible absorption spectra of Pd/C-TiO_2, which possess a strong absorption band in the near-infrared region (Figure 4). Recently, near-infrared-activated photocatalysts have generated extensive interest among researchers.[32–34] Defects induced a new energy-level structure in photocatalysts such as Bi_2WO_6 have been proposed as an important reason for the enhanced infrared-activated photocatalytic activity. Herein, Pd/C-TiO_2 is put forward as a potential near-infrared-activated photocatalyst, possibly owing to the semiconductor properties of small-sized ((1.6$\pm$0.5) nm) Pd nanoparticles that is caused by the quantum-size effect.[35]

On the basis of the above results, the mechanisms of the enhanced photocatalytic activity are proposed (Figure 6).

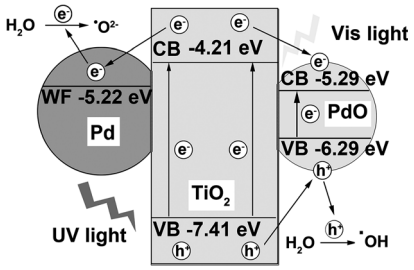

Figure 6. Illustration of the possible mechanisms of electron–hole separation and energy-band matching for PdO/C-TiO_2 and Pd/C-TiO_2 heterostructured nanobelts.

Clearly, the formation of a conformal contact between the C-TiO_2 nanobelts and PdO or Pd nanoparticles is a prerequisite for improving the photocatalytic performance. In the case of PdO/C-TiO_2 nanobelts, energy-band matching and the P–N junction effect play important roles in reducing the electron/hole (e^-/h^+) recombination rate and enhancing the quantum yield. PdO has been reported as a p-type semiconductor with bandgap values from 0.1 to 2.7 eV.[36,37] Both the conduction band (−5.27 eV) and the valence band (−6.29 eV) of PdO nanoparticles lie between those of TiO_2 nanobelts (−4.21 versus −7.41 eV). Therefore, the photoinduced electron transfer that occurs from TiO_2 nanobelts to PdO nanoparticles prolongs the lifetime of photoelectron–hole pairs. By comparison, the enhanced photocatalytic activity for Pd/C-TiO_2 nanobelts can be ascribed to the Schottky barrier effect that features a higher potential gradient. The Schottky barrier produced at a metal–semiconductor interface serves as an efficient electron trap, thereby retarding the electron–hole (e^-/h^+) recombination process. Finally, it is widely accepted that PdO is a more effective electron acceptor than Pd,[37,38] which further contributes to its enhanced photocatalytic activity. Under visible-light irradiation, the plasmonic and quantum-size effect were determined to be the main reasons for the enhanced photocatalytic activity of Pd/C-TiO_2. As for PdO/C-TiO_2, the enhanced performance was attributed to the sensitizing effect of the PdO nanoparticles.

Conclusion

In summary, PdO/C-TiO_2 and Pd/C-TiO_2 heterostructured nanobelts are constructed by growing small and uniform loaded PdO ((1.3$\pm$0.4) nm) and Pd ((1.6$\pm$0.5) nm) nanoparticles on the surface of TiO_2 nanobelts. The heterostructure can dramatically enhance the photocatalytic activity of C-TiO_2 nanobelts by modulating the separation and transport of the photocharge. Among the TiO_2 nanobelts (i.e., C-TiO_2 nanobelts, and PdO/C-TiO_2 and Pd/C-TiO_2 heterostructured nanobelts), PdO/C-TiO_2 exhibits the highest photocatalytic activity under UV and visible-light irradiation. The enhanced photocatalytic activity of PdO/C-TiO_2 and Pd/C-TiO_2 nanobelts is attributed to the energy-band matching and P–N junction effect for PdO/C-TiO_2 nanobelts and the Schottky barrier effect for Pd/C-TiO_2 nanobelts, respectively, under UV-light irradiation. Under visible-light irradiation, the plasmonic and quantum-size effect of Pd/C-TiO_2 were observed.

Experimental Section

General

Titania P25 (TiO_2; ca. 80% anatase and 20% rutile), sodium hydroxide (NaOH), hydrochloric acid (HCl), sulfuric acid (H_2SO_4), palladium chloride ($PdCl_2$), sodium borohydride ($NaBH_4$), and sodium sulfate (Na_2SO_4) were purchased from the China National Medicines Corporation Ltd. All chemicals were of analytical grade without further purification. Deionized water was used throughout this study.

Preparation of TiO_2 Nanobelts

Hydrogen titanate ($H_2Ti_3O_7$) nanobelts were synthesized by a modified literature report[23] through the hydrothermal process in 10 M NaOH aqueous solution at 180 °C for 72 h. The as-obtained $H_2Ti_3O_7$ nanobelts were acid-corroded by hydrothermal treatment at 100 °C for 8 h with an aqueous solution of H_2SO_4 (0.02 M). By annealing the acid-corroded hy-

drogen titanate nanobelts at 600 °C for 2 h, anatase TiO_2 nanobelts with a rough surface were obtained, which was referred to as C-TiO_2.

PdO/C-TiO_2 and Pd/C-TiO_2 Nanobelt Heterostructures

PdO/C-TiO_2 nanobelt heterostructures (2 wt %) were prepared by a deposition–precipitation method. C-TiO_2 nanobelts (0.15 g) were added to distilled water (50 mL), and the suspension was sonicated for 30 min. Then $PdCl_2$ (7.68 mL, 5.64 mmol L^{-1}) solution was added to the suspension, and the mixture was stirred for 30 min. Subsequently, NaOH solution (0.1 mol L^{-1}) was slowly added to the resulting mixture. In this process, the sol-like PdO adsorbed onto the surface of C-TiO_2 nanobelts at about pH 7, thus leading to homogeneously dispersed PdO nanoparticles. The light yellow product (PdO/C-TiO_2) was filtered, washed with water, and dried at 70 °C for 12 h. As for Pd/C-TiO_2, prior to centrifugation of the PdO/C-TiO_2 suspension, the superfluous $NaBH_4$ aqueous solution (0.01 mol L^{-1}) was slowly added into the PdO/C-TiO_2 suspension. The PdO nanoparticles on the surface of C-TiO_2 nanobelts were reduced to Pd nanoparticles by $NaBH_4$. The suspension changed from light yellow to gray. The gray solution was retained after several washings with deionized water. Finally, the product was filtered and dried at 70 °C for 12 h.

Characterization

XRD patterns of catalysts were recorded with a Bruker D8 Advance powder X-ray diffractometer with $Cu_{K\alpha}$ radiation ($\lambda = 0.15406$ nm). A Hitatchi S-4800 field-emission scanning electron microscope was used to characterize the morphologies and size of the synthesized samples. The chemical composition was investigated by means of energy-dispersive X-ray spectroscopy (EDS). TEM images were taken with a JOEL JEM 2100F microscope. UV-visible absorption spectra of the samples were recorded with a UV/Vis spectrophotometer (UV-2550, Shimadzu) with an integrating sphere attachment. The analyzed range was 200–800 nm, and $BaSO_4$ was used as a reflectance standard. XPS was performed with an ESCALAB 250 instrument.

Evaluation of Photocatalytic Activity under UV and Visible-Light Irradiation

Methyl orange (MO; 20 mg L^{-1}), methylene blue (MB; 25 mg L^{-1}), rhodamine B (15 mg L^{-1}), and *p*-chlorophenol (20 mg L^{-1}) were selected as model chemicals to evaluate the activity and properties of the as-prepared photocatalysts. In a typical experiment, aqueous suspensions (20 mL) of MO and photocatalyst powders (20 mg) were placed in a 50 mL beaker. Prior to the irradiation, the suspensions were stirred in the dark for 30 min to establish adsorption/desorption equilibrium between the dye and catalysts under ambient conditions. A 350 W mercury lamp with a maximum emission at 356 nm was used as the UV resource for UV-light photocatalysis. A 300 W Xe arc lamp through a UV cutoff filter ($\leq$420 nm) was used as the visible-light source for photocatalysis. At different irradiation intervals, the reaction solution was collected, then centrifuged to remove the catalyst, which was used to measure the concentration of MO by monitoring the absorbance with a UV/Vis spectrophotometer (UV-2102PC).

Photocurrent Measurements

For the fabrication of the photoelectrodes, ethanol suspensions (1 mL) of as-prepared photocatalyst powders (20 mg) were coated on indium–tin oxide (ITO) glass with the cover area of 1 cm^2 and allowed to dry under ambient conditions. The photocurrents were measured with an electrochemical workstation (CHI 750E, CH Instruments Inc., Shanghai) by using a three-electrode mode in 1 M Na_2SO_4 aqueous solution. The reference electrode and counter electrode were Ag/AgCl electrode (saturated KCl) and platinum wire, respectively. The as-prepared photoelectrodes were used as the anodes for electrochemical characterizations. A 350 W mercury lamp with a maximum emission at 356 nm was used as the UV resource with a light intensity of 900 mW cm^{-2}. A 300 W Xe arc lamp through a UV cutoff filter ($\leq$420 nm) was used as the visible-light source with a light intensity of 650 mW cm^{-2}. The monochromatic light of 450 (208), 550 (215), and 650 nm (228 mW cm^{-2}) were obtained from a 300 W Xe arc lamp by monochromatic light filter.

Acknowledgements

This research was supported by the National Natural Science Foundation of China (50925205), the "100 Talents Program" of the Chinese Academy of Sciences, the Recruitment Program of Global Experts, the PhD Start-up Funds of the Natural Science Foundation of Guangdong Province (S2013040016465), Zhujiang New Stars of Science and Technology, and the Fundamental Research Funds for Central Universities, China.

[1] T. S. Kang, A. P. Smith, B. E. Taylor, M. F. Durstock, *Nano Lett.* **2009**, *9*, 601–606.
[2] C. S. Pan, D. S. Zhang, L. Y. Shi, J. H. Fang, *Eur. J. Inorg. Chem.* **2008**, 2429–2436.
[3] Y. Cheng, P. Xiong, C. S. Yun, G. F. Strouse, J. P. Zheng, R. S. Yang, Z. L. Wang, *Nano Lett.* **2008**, *8*, 4179–4184.
[4] R. S. Yang, Z. L. Wang, *J. Am. Chem. Soc.* **2006**, *128*, 1466–1467.
[5] G. C. Xi, S. X. Ouyang, P. Li, J. H. Ye, Q. Ma, N. Su, H. Bai, C. Wang, *Angew. Chem. Int. Ed.* **2012**, *51*, 2395–2399; *Angew. Chem.* **2012**, *124*, 2445–2449.
[6] Y. Li, B. Tan, Y. Wu, *Nano. Lett.* **2008**, *8*, 265–270.
[7] X. W. Xie, Y. Li, Z. Q. Liu, M. Haruta, W. J. Shen, *Nature* **2009**, *458*, 746–749.
[8] B. Liu, E. S. Aydil, *J. Am. Chem. Soc.* **2009**, *131*, 3985–3990.
[9] W. J. Zhou, H. Liu, J. Y. Wang, D. Liu, G. J. Du, J. J. Cui, *ACS Appl. Mater. Interfaces* **2010**, *2*, 2385–2392.
[10] N. Q. Wu, J. Wang, D. N. Tafen, H. Wang, J. G. Zheng, J. P. Lewis, X. G. Liu, S. S. Leonard, A. Manivannan, *J. Am. Chem. Soc.* **2010**, *132*, 6679–6685.
[11] F. W. Zhuge, J. J. Qiu, X. M. Li, X. D. Gao, X. Y. Gan, W. D. Yu, *Adv. Mater.* **2011**, *23*, 1330–1334.
[12] F. Shao, J. Sun, L. Gao, S. W. Yang, J. Q. Luo, *J. Mater. Chem.* **2012**, *22*, 6824–6830.
[13] J. Nisar, Z. Topalian, A. D. Sarkar, L. Österlund, R. Ahuja, *ACS Appl. Mater. Interfaces* **2013**, *5*, 8516–8522.
[14] P. G. Hu, G. J. Du, W. J. Zhou, J. J. Cui, J. J. Lin, H. Liu, D. Liu, J. Y. Wang, S. W. Chen, *ACS Appl. Mater. Interfaces* **2010**, *2*, 3263–3269.
[15] W. J. Zhou, H. Liu, R. I. Boughton, G. J. Du, J. J. Lin, J. Y. Wang, D. Liu, *J. Mater. Chem.* **2010**, *20*, 5993–6008.
[16] J. Wang, D. N. Tafen, J. P. Lewis, Z. L. Hong, A. Manivannan, M. J. Zhi, M. Li, N. Q. Wu, *J. Am. Chem. Soc.* **2009**, *131*, 12290–12297.
[17] N. J. Borys, M. J. Walter, J. Huang, D. V. Talapin, J. M. Lupton, *Science* **2010**, *330*, 1371–1374.
[18] Z. Y. Tang, N. A. Kotov, M. Giersig, *Science* **2002**, *297*, 237–240.
[19] L. Liu, X. Gua, C. Sun, H. Li, Y. Deng, F. Gao, L. Dong, *Nanoscale* **2012**, *4*, 6351–6359.
[20] Z. Y. Liu, D. D. Sun, P. Guo, J. O. Leckie, *Nano Lett.* **2007**, *7*, 1081.
[21] W. J. Zhou, Z. Y. Yin, Y. P. Du, X. Huang, Z. Y. Zeng, Z. X. Fan, H. Liu, J. Y. Wang, H. Zhang, *Small* **2013**, *9*, 140–147.
[22] J. Cao, J. Z. Sun, H. Y. Li, J. Hong, M. Wang, *J. Mater. Chem.* **2004**, *14*, 1203–1206.
[23] W. J. Zhou, G. J. Du, P. G. Hu, G. H. Li, D. Z. Wang, H. Liu, J. Y. Wang, R. I. Boughton, D. Liu, H. D. Jiang, *J. Mater. Chem.* **2011**, *21*, 7937–7945.
[24] E. Formo, E. Lee, D. Campbell, Y. N. Xia, *Nano Lett.* **2008**, *8*, 668–672.
[25] C. Jiang, S. Ranjit, Z. Duan, Y. L. Zhong, K. P. Loh, C. Zhang, X. Liu, *Nanoscale* **2009**, *1*, 391–394.
[26] A. Kolmakov, D. O. Klenov, Y. Lilach, S. Stemmer, M. Moskovits, *Nano Lett.* **2005**, *5*, 667–673.
[27] H. L. Wang, Y. Y. Liang, Y. G. Li, H. J. Dai, *Angew. Chem. Int. Ed.* **2011**, *50*, 10969–10972; *Angew. Chem.* **2011**, *123*, 11161–11164.
[28] K. Awazu, M. Fujimaki, C. Rockstuhl, J. Tominaga, H. Murakami, Y. Ohki, N. Yoshida, T. Watanabe, *J. Am. Chem. Soc.* **2008**, *130*, 1676–1680.
[29] S. K. Cushing, J. T. Li, F. K. Meng, T. R. Senty, S. Suri, M. J. Zhi, M. Li, A. D. Bristow, N. Q. Wu, *J. Am. Chem. Soc.* **2012**, *134*, 15033–15041.

[30] K. F. Wu, W. E. Rodríguez-Córdoba, Y. Yang, T. Q. Lian, *Nano Lett.* **2013**, *13*, 5255–5263.
[31] S. Mubeen, J. Lee, N. Singh, S. Krämer, G. D. Stucky, M. Moskovits, *Nat. Nanotechnol.* **2013**, *8*, 247–251.
[32] W. P. Qin, D. S. Zhang, D. Zhao, L. L. Wang, K. Z. Zheng, *Chem. Commun.* **2010**, *46*, 2304–2306.
[33] G. Wang, B. B. Huang, X. C. Ma, Z. Y. Wang, X. Y. Qin, X. Y. Zhang, Y. Dai, M. H. Whangbo, *Angew. Chem. Int. Ed.* **2013**, *52*, 4810–4813; *Angew. Chem.* **2013**, *125*, 4910–4913.
[34] J. Tian, Y. H. Sang, G. W. Yu, H. D. Jiang, X. N. Mu, H. Liu, *Adv. Mater.* **2013**, *25*, 5075–5080.
[35] X. Q. Huang, S. H. Tang, X. L. Mu, Y. Dai, G. X. Chen, Z. Y. Zhou, F. X. Ruan, Z. L. Yang, N. F. Zheng, *Nat. Nanotechnol.* **2011**, *6*, 28–32.
[36] K. C. Hass, A. E. Carlsson, *Phys. Rev. B* **1992**, *46*, 4246–4249.
[37] Q. Li, Y. W. Li, P. G. Wu, R. C. Xie, J. K. Shang, *Adv. Mater.* **2008**, *20*, 3717–3723.
[38] Q. Li, W. Liang, J. K. Shang, *Appl. Phys. Lett.* **2007**, *90*, 063109.

Received: December 10, 2013
Revised: February 18, 2014
Published online: April 22, 2014